Nanowire iron(III) coordination polymer based on 1,2,4-triazolo[1,5-*a*]pyrimidine and chloride ligands

Piera Sabatino,*[a] Simone D'Agostino,[a] Jacopo Isopi,[a] Simona Rubino,[b] Massimo Marcaccio,[a] Maria Assunta Girasolo*[b]

[a] *University of Bologna, Department of Chemistry G. Ciamician, via F. Selmi 2, 40126 Bologna, Italy*

[b]*University of Palermo, Department of Biological, Chemical and Pharmaceutical Sciences and Technologies (STEBICEF), Viale delle Scienze Ed.17, 90128 Palermo, Italy*

*Corresponding author.
E-mail address: piera.sabatino@unibo.it (P.Sabatino), assunta.girasolo@unipa.it (M.A.Girasolo)

Abstract

The neutral ligand 1,2,4-triazolo[1,5-*a*]pyrimidine (**tp**) has been employed to prepare a new coordination compound of Fe(III), $[FeCl_3(tp)_2]_n$ (**1**). Compound **1** was investigated by single crystal X-ray diffraction and found to be a coordination polymer forming a ladder structure based on metal-ligand interactions, while H-bonding and aromatic interactions contribute to the supramolecular self-assembly into a 3D nanostructured material. The polymeric assembly is retained also in solution, where a metallo-supramolecular polymer based on coordinative metal-ligand binding is present, as shown by Dynamic Light Scattering (DLS) measurements. The redox properties of the Fe(III) coordination polymer have also been investigated in different solvents and its nanowire structure has been assessed by Atomic Force Microscopy (AFM) imaging of the species deposited onto a freshly cleaved mica surface.

Keywords: 1,2,4-triazolo[1,5-*a*]pyrimidine; solid state structure; cyclic voltammetry, self-assembly, scanning probe microscopy.

1. Introduction

1,2,4-triazole and its derivatives represent an important class of heterocycles, which are very useful ligands in coordination chemistry. The use of the 1,2,4-triazole moiety as part of a ligand system in metal complexes has gained considerable attention in recent years [1,2]. It is well known that 1,2,4-triazoles exhibit different tautomeric forms and 1,2,4-triazolo[1,5-*a*]pyrimidines present structures similar to purine, but with a pyrimidine nitrogen atom in a bridgehead position and disappearance of the acidic H-atom of the five-membered ring. The similarity between the two systems allows to consider the coordination compounds of 1,2,4-triazolo[1,5-*a*]pyrimidines as model systems for various naturally occurring metal coordination compounds. For instance, coordination compounds bidentate through N3 and N4 positions can act as model systems for adenine.

In addition, in a quite recent investigation on polar, extensively conjugated, planar heterocyclic compounds, the crystal structure of 1,2,4-triazolo-[1,5-*a*]pyrimidine was determined with the aim to explain its high vaporization enthalpy on the basis of possible intermolecular interactions [3]. Actually, the strong π-π stacking interactions shown in its crystal structure led to hypothesize their possible persistence in solution, making it an interesting ligand for coordination compounds [1].

Iron is an essential element in the majority of biological systems: oxo- hydroxo- and carboxylato-bridged polynuclear iron (III) units have been found in many non-heme metalloproteins and metalloenzymes [4]. It is present in many cellular processes, including energy production, electron transport and DNA synthesis due to its role as a co-factor for proteins such as oxidases, cytochromes and ribonucleotide reductase [5,6].

The earliest examples of iron(II) complexes with 1,2,4-triazole based ligands were reported by Haasnoot, Reedijk and co-workers in the mid-1980s [7], and have been recently reviewed by Feltham et al. [8]. While many transition metal triazolopyrimidine complexes have been

investigated with both monodentate and bridging N-donor ligands [2], to the best of our knowledge only one X-ray structure investigation of a Fe(II) two-dimensional polymer with N1,N3-bridging triazolopyrimidine ligands has been reported up to date [9a]. Interestingly, this seems to be the only example of triazolopyrimidine N1,N3-bidentate mode on iron centers generating a coordination polymer, as expected for this binding mode of the ligand. Much more common, for transition metals different from iron, is the bidentate mode through nitrogen atoms at positions 3 and 4 [2c]. Other coordination compounds of Fe(II) with triazolopyrimidine ligands are invariably monodentate as, for instance, in the octahedral complexes $[Fe(NCS)_3(dmtp)_2(H_2O)]$, $[Fe(NCS)_2(dmtp)_2(H_2O)_2]$ [9b] and $[Fe(NCS)_2(detp)_3(H_2O)]$ [10].

Mononuclear Fe(III) complexes with 1,2,4-triazole ligands, on the other hand, have been synthesized and investigated by X-ray crystallographic studies [11]; the octahedral cationic complex $[Fe(HL)_2]^+$, [H_2L = 3-(2-phenol)-5-(pyridin-2-yl)-1,2,4-triazole], has an O_2N_4 donor set with stereochemical and electronic requirements quite different from our compound. Therefore, our iron(III)-triazolopyrimidine compound is the first example presenting two different binding modes, namely both N3-monodentate and N3,N1-bridging, this latter mode giving rise to a coordination polymer, as already reported for Ni(II), Co(II) and Cu(I) complexes [2c].

Recently, synthesis and characterization of metallo-supramolecular polymers have been thoroughly reviewed by Winter and Schubert [12]. Compound $[FeCl_3(tp)_2]_n$ (**1)** appears, both in the solid state and in solution, a metallo-supramolecular polymer based on coordinative binding of the neutral N-rich triazolo-pyrimidine as multidentate ligand to the metal centers. We report here the characterization, DLS measurements and the crystal structure of the polymeric iron(III) compound **1**, together with its redox properties. Also, an AFM investigation of the self-assembling of **1** on two different kinds of surfaces has been carried out.

2. Experimental

2.1. Chemicals and instrumentation

All chemicals were reagent grade and were used without further purification. $FeCl_3$ and 1,2,4-triazolo[1,5-*a*]pyrimidine were purchased from Sigma-Aldrich. Electrochemical or analytical grade tetrabutylammonium hexafluorophosphate (TBAH) from Sigma-Aldrich was used as received as supporting electrolyte. Acetonitrile (ACN, from Sigma-Aldrich) and N,N-dimethylformamide (DMF, from Merck) were purified by distillation (ACN under argon and DMF under reduced pressure at 35 °C) and dried to remove water by storing the solvent over activated 4 Å molecular sieves in a specially designed Schlenk flask and protected from light.

Elemental microanalyses for C, H and N were performed at the Laboratorio di Microanalisi, University of Padova, Italy. Infrared spectra (nujol mulls, CsI windows) were recorded with an FT-IR spectrometer Perkin-Elmer Spectrum One.

2.2. Synthesis

A solution of the $FeCl_3$ (162 mg, 1 mmol) in ethanol (15 mL) was added to a solution of the ligand **tp** (360 mg, 3 mmol). The resulting orange solution was stirred for 2 h at room temperature. Upon slow evaporation, from the ethanol solution, bright red crystals of **1** were obtained, which were collected by filtration. Anal. Calc. for $C_{10}H_8N_8FeCl_3$ (MW = 402.43g/mol) C, 29.85; H, 2.00; N, 27.85; Cl, 26.43. Found: C, 29.88; H, 2.19; N, 27.95; Cl, 26.32. IR (nujol, cm^{-1}): 1614 ν_{tp}, 1535 and 1511 ν_{py}.

2.3. X-ray crystal structure determination

Details of crystal data and refinement are given in Table1. Preliminary examination data and data collection were carried out on an Oxford Supernova CCD detector at 100K with Mo-Kα radiation, λ= 0.71073 Å, monochromator graphite.

Data reduction was automatically performed by CrysAlisPRO (Oxford Diffraction Ltd., UK). The cell parameters were obtained and refined using the PHICHI [13] and DIRAX [14] programs,

respectively, catching reflections with random orientation in *hkl* planes. Intensities were corrected by Lorentz polarization and absorption with the SADABS [15] program. The XPREP [16] program was used for analysis of the data reduction and revealed a monoclinic-*C2/c* space group.

The structure of compound **1** was solved by direct methods using the SHELXS-97 program [17]. SHELXL-97 [18] was used for structure solution and refinement based on F^2. Anisotropic thermal vibrations were applied to all atoms. Hydrogen atoms bound to carbon atoms were added in calculated positions. Aromatic carbon atoms were refined with Uiso(H) = 1.2 Ueq C sp^2 and methyl carbon atoms with Uiso(H) = 1.5 Ueq C sp^3. Final R indexes for 200 parameters refined were: R1 = 0.0427 for 1638 Fo > 4sig(Fo) and 0.1174 for all 3234 data, wR2 = 0.104, GooF = S = 0.927 for all data. Molecular graphics were prepared using Mercury CSD 3.10.2 [19].

2.4. Dynamic Light Scattering (DLS) measurements

DLS measurements were performed on a Malvern Nano ZS system with a 532 nm laser beam and a fixed detection angle of 173° on a small amount of both ligand and compound **1**. Samples were dissolved in distilled H_2O upon sonication, housed in disposable polystyrene cuvettes of 1 cm optical path lengths and analyzed [20]. The width of DLS hydrodynamic diameter distribution is indicated by PdI (Polydispersion Index). In case of a mono-modal distribution (Gaussian) calculated by means of cumulative analysis, PdI=(σ/Zavg)2, where σ is the width of the distribution and Zavg is average diameter of the particles population.

2.5. Electrochemistry

Electrochemical experiments were carried out using both ACN and DMF as solvents and TBAH as electrolyte, in an air-tight single-compartment cell equipped with platinum working and counter electrodes and a reference electrode. The reference electrode was either an aqueous saturated calomel electrode (SCE) or a silver spiral as a quasi-reference, calibrated by adding ferrocene (Fc), at the end of each experiment, as an internal standard and measuring them with

respect to the ferrocinium/ferrocene couple ($Fc^{+/0}$) standard potential (which is +0.58 V vs SCE) [21]. The drift of such a quasi-reference electrode was negligible during the time required for an experiment. All the $E_{½}$ potentials have been directly obtained from cyclic voltammetric curves as averages of the cathodic and anodic peak potentials and by digital simulation in the case of non-Nernstian or overlapping processes.

The cell containing the supporting electrolyte was dried and deareated under vacuum at 100 °C for about 3 hours before each experiment. The solvent was transferred into the cell by cannula procedure under Ar. The species under examination was added to the electrolyte solution immediately before performing the experiment.

Voltammograms were recorded with a custom made fast potentiostat [22] controlled by an AMEL Mod. 568 programmable function generator. The potentiostat was interfaced to a Nicolet Mod. 3091 digital oscilloscope and the data transferred to a personal computer by the program Antigona [23]. Minimization of the uncompensated resistance effect in the voltammetric measurements was achieved by the positive-feedback circuit of the potentiostat. Digital simulations of the cyclic voltammetric curves were carried out either by Antigona or DigiSim 3.0 (Bioanalytical Systems, Inc.), utilizing a best fitting procedure of the experimental curves recorded at different scan rates spanning over, at least, two orders of magnitude [21].

AFM imaging and analysis were performed in air with a Digital NanoScope 3D Multimode microscope (Veeco, USA) using phosphorus n-doped Silicon probes (spring constant, 20-80 N/m; resonance frequency 290-330 kHz; nominal tip radius <10 nm) and operating in tapping mode. Samples for the AFM experiments were prepared by either spin-coating or drop-casting a solution of iron-polymer complex **1** in THF (1 mg/ml) both on p-type Si/SiO_2 wafer and freshly cleaved mica surface (obtained by peeling with sellotape). The images were obtained by optimizing the setpoint tapping amplitude with respect to the free amplitude of the probe, near the resonance frequency of the probe itself, as reported elsewhere [24].

3. Results and Discussion

3.1. Infrared spectra

Compound **1** has been characterized by FT-IR spectroscopy ~~and its crystal structure has been investigated by single crystal X-ray diffraction studies (see Table 1)~~. IR spectra of compound **1** were measured in the 4000-400 cm^{-1} region. The two most characteristic bands of the **tp** ligand [25], are assigned to an overall triazolopyrimidine and pyrimidine ring mode vibrations *i.e.* ν_{tp} (1621cm^{-1}) and ν_{py} (1533 and 1515 cm^{-1}). In the compound **1**, the bands are found at 1614 cm^{-1} (ν_{tp}), and 1535 and 1511 cm^{-1} (ν_{py}), respectively.

3.2. Crystallography

Compound **1** was isolated as crystals suitable to be studied by single-crystal X-ray diffraction. The crystal and molecular structure of compound **1** is shown in Fig. 1, together with its crystallographic labelling; Figure 2 shows its molecular packing, while selected bond lengths and angles are listed in Table 2.

The iron(III) centre is in an octahedral environment formed by three chloride ions and three **tp** ligands, two of which are symmetry-related and behave as μ^2-bridging ligands at the triazolo moiety with two symmetry related Fe ions through their N(1) and N(3**)** atoms, respectively, generating polymeric chains of *mer*-isomers. Actually, only one monodentate **tp** ligand bonded at the iron centre at N(3A) and one bridging **tp** ligand binding at N(3B) constitute the asymmetric crystallographic unit together with the $FeCl_3$ moiety, while the third **tp** moiety, binding at N(1B), is generated from the previous one by means of a glide plane along the *b*-axis (symm op. 0.5000-x, -0.5000+y, 0.5000-z). The **tp** ligands engage at most two N atoms in metal coordination in the μ^2-bridging ligands and Fe-N bond distances are the following: Fe–N(3B) = 2.2653(0.0033), Fe-N(1B) = 2.2029 (0.0031), Fe-N(3A) = 2.1410 (0.0032) Å, where the longer bond distance belongs to a **tp** ligand *trans* to Cl(3) but bidentately coordinated and the shorter one is displayed for a monodentate

ligand, *trans* to a (glide plane) symmetry-related bidentate **tp**. Comparison of these values with those present in poly-bis(thiocyanato-*N*)-bis-μ-[1,2,4]triazolo[1,5-*a*]pyrimidine-N^1,N^3)iron(II) [9a] gives a second evidence, apart from the crystals bright colour (see Experimental section), of the oxidation state at the metal centre. In fact, Fe-N bond lengths with the **tp** ligand in the Fe(II) complex are significantly longer, varying in the range 2.25(2) and 2.33(2) Å, according to the different metal electronic environment.

Interestingly, the greater Fe-Cl bond distance [Fe-Cl(2) 2.3450 (0.0012)] is significantly longer than both Fe-Cl(1) 2.2703(0.0011) Å and Fe-Cl(3), 2.2883 (0.0015), being *trans* to the former and, very likely, more prone to hydrolysis with respect to Cl(1), due to its minor involvement in H-bonding [see later].

A crude simulation "in silico" of the rotation around the single Fe-N(3A) bond accomplishes to bring N(4A) close enough [ca. 3 Å] to the iron atom with which it shares the bridging triazolo-pyrimidine ligand [Fe(i)], possibly switching the coordination of the monodentate ligand towards that of a bridging moiety. In that case, a different mode of coordination involving both N(3) and N(4) atoms, and excluding N(1), will be exploited with respect to the other bridging ligand: that is from both the triazole, N(3), and the pyrimidine, N(4), ring, resembling the bidentation mode shown by transition metals different from iron (see discussion above). On the assumption that all the three N functionalities would be involved in different ways of interaction with the iron atom: a possible increase in the number of donor N-atoms that bind to the metal as bridging moieties, instead of monodentate ones, could further contribute to the polymeric complex stability [12]. Electrochemical data, in the following section, validate that hypothesis.

Fe(III) centers involved in ligands sharing are positioned only 6.20 Å apart (for the closest neighbour at –x+1/2, y+1/2, -z+1/2. In $[Fe(NCS)_2(tp)_2]$, the analogous Fe^{II}-Fe^{II} distance in the layers is much longer, i.e. 6.46 Å [9a].

An extensive network of intermolecular H-bonding of CH…N kind among triazolo and pyrimidine moieties of the bridging **tp** units and CH…Cl kind to both bridging and monodentate **tp**

units contribute to the packing pattern and self-assembly of **1,** with different motives for the three Cl atoms. Actually Cl(1) forms a bidentate H-bonding with two pyrimidine rings of bridging **tp** moieties, Cl(2) only connects to a pyrimidine ring of a monodentate **tp**, while Cl(3) is H-bonded to either triazolo (intermolecular) and pyrimidine (intramolecular) rings belonging to bridging **tp** units.

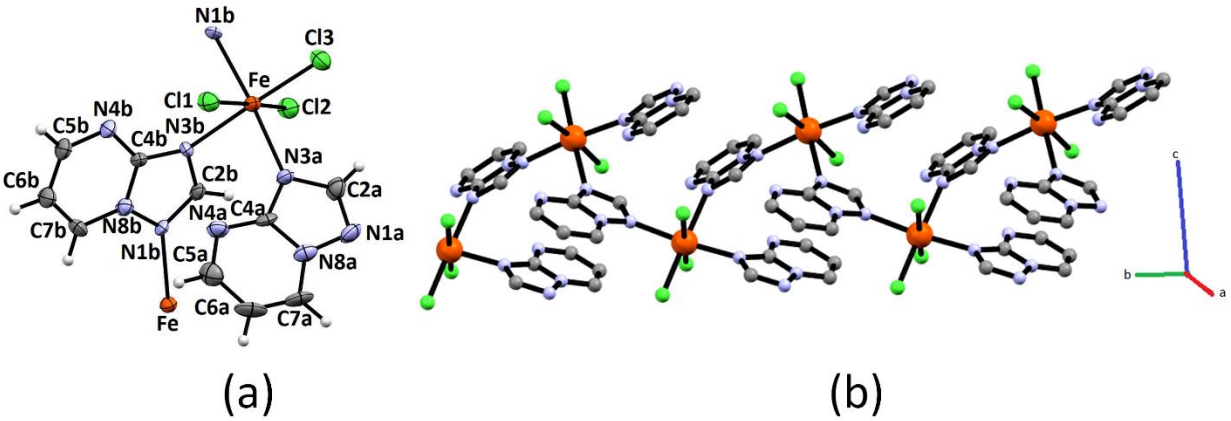

Fig. 1 a) The asymmetric unit for **1**, showing the atomic crystallographic numbering scheme. Displacement ellipsoids are drawn at the 50% probability level. **b**) Infinite chain of **1** as viewed along the *a* axis.

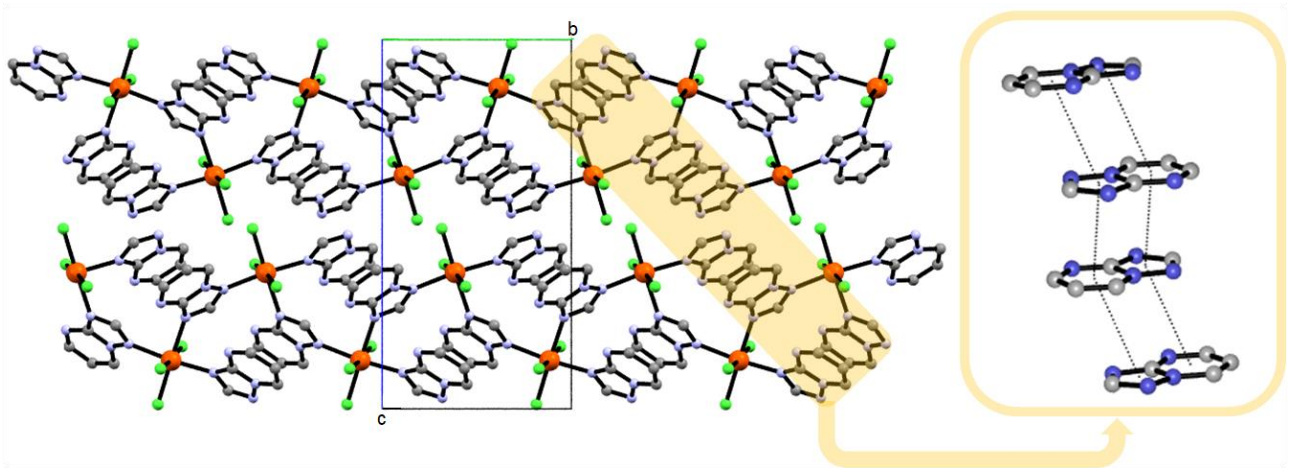

Fig. 2 Packing of **1**. In the close-up, right, head-to-tail π-stacking is shown.

The H-bonding scheme adds up to face-to-face and edge-to-face π-interactions involving triazole and pyrimidine rings of **tp** ligands (about 3.72 Å) with an head-to-tail recognition motif (inset of

Fig. 2) different from the head-to-head shown by the ligand alone [3], forming layers of stacked aromatic rings and generating the 3D supramolecular network (Fig. 2).

The ladder structure formed by the coordination iron polymer and based on iron-ligand interactions extends along the crystallographic *b* axis, while the connections between the ladders, formed by H-bonding and π-π stacking interactions, dominate along the *c* direction (shown in blue, Fig. 1).

Calculation of empty spaces big enough to hold a small spherical probe of 0.5 Å in radius sums up to a 10% of the total volume in the unit cell, giving an estimate of the volume which can be filled by solvent or guest molecules. Thus, the metallo-supramolecular assembly may be easily fine-tuned generating, for instance, opportune nanocavities by using either a reorganized coordination sphere around iron or ligands of different size, but same versatility of **tp**, as linkers between the iron atoms. In addition, the nanostructured material can be used as a precursor towards building of opportunely tailored iron nanowires and/or for the efficient fabrication of metal nanoparticles.

3.3 DLS analysis

DLS analysis was performed in order to confirm the persistence of the nanosized aggregates in solution and evaluate the nanoparticles hydrodynamic diameters. DLS obtains the nanoparticle size information by measuring the diffusion coefficient of the particle [26], its "hydrodynamic" dimension. The diffusion coefficient of a particle is not only dependent on its size, but also on the shape and the surface chemistry of the particles because these parameters affect the particle–solvent interactions, and therefore, the Brownian motion of the particles.

The DLS experimental measurements show that our samples are characterized by a rather high PdI, an indication that several diameter distributions are present in suspension. As an intensity based technique, DLS overestimate the presence of larger diameter populations and therefore a discussion of the DLS results in terms of number distribution rather than intensity distribution offer a more realistic picture of the main distributions that are present within the ligand and complex **1** samples (Fig. 3)

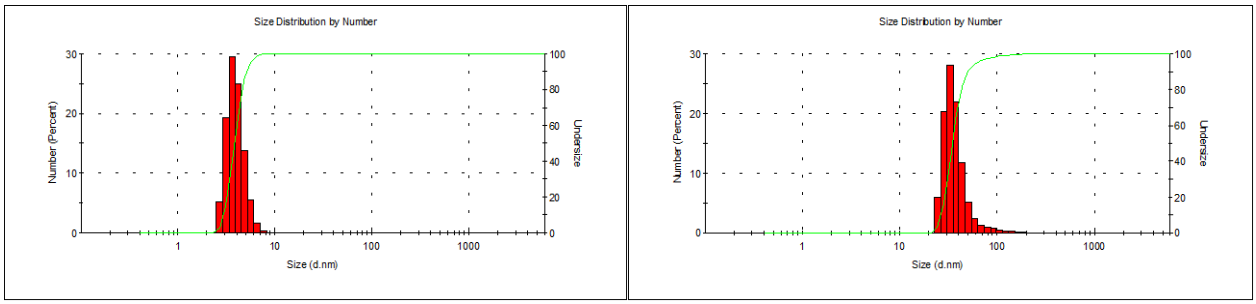

(a) (b)

Fig. 3 Size distribution by number of compound **1** (a) (dNUMBER MEAN = (3.9 ± 0.2) nm; PdI = 0.63) and ligand (b) (dNUMBER MEAN = (41 ± 3) nm; PdI = 0.33) suspension obtained by DLS analysis.

These results show that the main population has greater dimensions for the ligand than for compound **1**. This is in agreement with the increase of the average hydrodynamic diameter obtained from distributions by intensity, and with the scattering signal measured by the detector. The formation of the coordination polymer seems to affect the strong p-π stacking interactions shown by the ligand, probably because the coordination environment produced by the presence of the metal ions release the aromatic rings interactions. As in the case of nanorods, perhaps the shape and the surface chemistry of the nanoaggregates affect their translational diffusion coefficient more than their mass, the DLS results depending more on the morphology of the polymeric aggregates

Our samples, however, are characterized by a rather high polydispersion, therefore we prefer to describe DLS results in terms of number distribution rather than intensity distribution, comparing ligand and complex **1 (Fig. 3)**

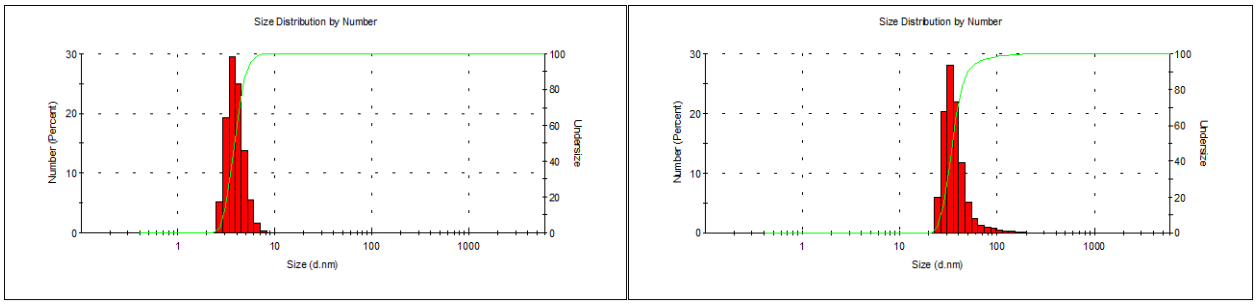

(a) **(b)**

Fig. 3 Size distribution in number of both **1** (a) and ligand (b) by DLS analysis.

The observed results show that the main population has greater dimensions for the ligand than complex **1**, in agreement with the increase of the average hydrodynamic diameter obtained from intensity data and scattering signal to detector. The formation of the coordination polymer seems to affect the strong π-π stacking interactions shown by the ligand, towards a looser arrangement of the aromatic rings probably dictated by the coordination environment.….

As in the case of nanorods, perhaps the shape and the surface chemistry of the nanoaggregates affect their translational diffusion coefficient more than their mass, the DLS results depending more on the morphology of the polymeric aggregates.

3.4. Electrochemistry and Surface Analysis

The redox behavior of the polymeric species **1** has been investigated by cyclic voltammetry both in ACN and DMF. The cyclic voltammetric curve in ACN is reported in Fig. 4a (black trace: 1st cycle) and it shows a chemical and electrochemically irreversible electron transfer, with a redox potential of 0.15 V (*vs.* Ag/AgCl). The open circuit potential (OCP) of the fresh solution is 0.20 V; on the basis of the Nernst equation such a value is compatible with the oxidized form of the species (i.e., Fe^{III}).

The analysis of the voltammetric curves, recorded at different scan rates (comprised between 0.2 V/s and 20 V/s), evidences a sluggish electron transfer process complicated by some kind of chemical reaction of the reduced species. Moreover, on the second cycle (red trace in Fig. 4a) the cathodic peak appears broader and less pronounced which typically happens when the electrode surface is partially passivated, by the products of the following up reaction, and the electron transfer processes has a low heterogeneous constant.

The simulations of the cyclic voltammetric curves at different sweep rates, over a range of two orders of magnitude, with an ECE mechanism (electrochemical step followed by a chemical reaction and a further electrochemical one) fit reasonably well the experimental results, thus

allowing to determine the E° value of the primary redox process (E°= 0.15 V), together with its heterogeneous electron transfer constant, which is $(9\pm1)\times10^{-4}$ cm/s) (Fig. S1 and Scheme S1). The electron transfer barrier is not perfectly symmetric (α = 0.7), thus indicating that the process involves a possible important structural change, as for example the outgoing of a chloride ligand. This could lead to a reorganization of the coordination sphere of the Fe-centre, due to the available uncoordinated nitrogens of the triazolo-pirimidine ligands.

In this respect, it is worth to note that the subsequent voltammetric cycle, after the first scan, lead to changes of the voltammetric pattern, as shown in Fig. 4a (2^{nd} cycle: red trace) and with much more evidence the multicycle voltammetric curves recorded in Fig. 4b. It can be seen that a second process starts to develop at about -1 V. Such a further reduction can be attributed to the product of the chemical reaction following the first reduction process and it can be hypothesized that this is the Fe-polymer that has undergone Cl^- loss. The chemical reaction following the electron transfer is an equilibrium process with a small forward kinetic constant (0.1 s^{-1}).

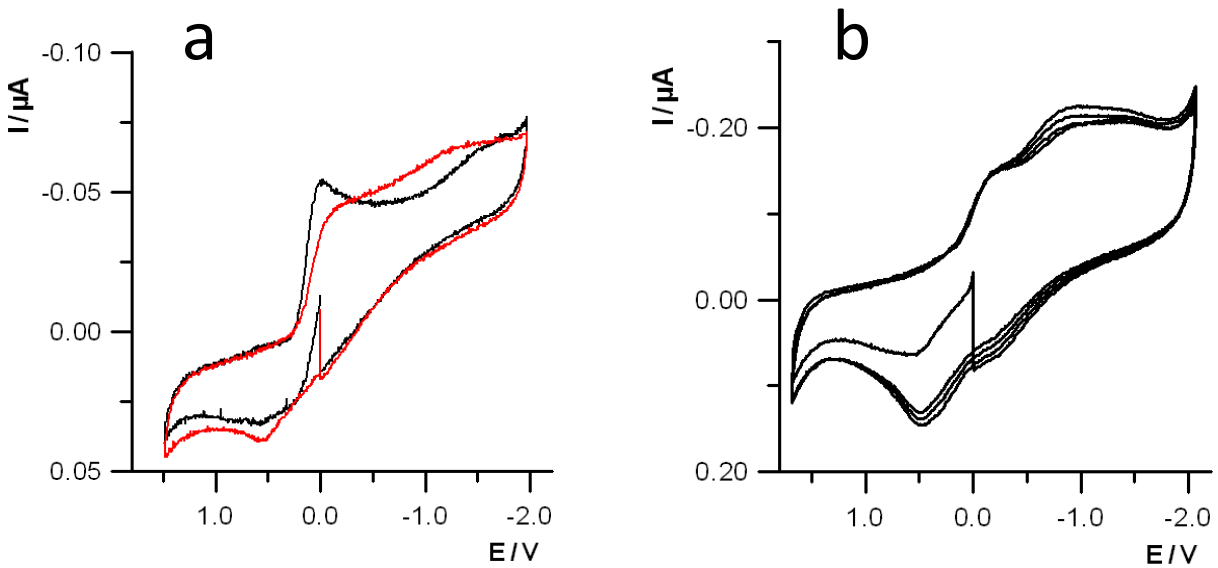

Fig. 4 Cyclic voltammetric curves of Fe-polymer **1** in 0.1 M TBAH/ACN. T=25 °C; (a) scan rate= 1 V/s, 1^{st} cycle: black curve, 2^{nd} cycle: red curve; (b) scan rate= 5 V/s.

It should also be noted that, as further experimental support to the possible involvement of ~~the~~ chloride outgoing in the redox process, the solutions (both in ACN and DMF) of the Fe-polymer species exposed to metal silver surfaces show deposition of AgCl on a silver wire, a clear evidence of chloride outgoing. However, scanning the potential at positive values, corresponding to the oxidation of Cl^-, no clear voltammetric evidences could be obtained.

As the polymeric compound **1** can be considered as a linearly extended molecular wire, it is also worth studying its assembling capabilities on a surface by scanning probe microscopy. In particular, a solution of the species **1** was spin-coated on two different, morphologically flat, types of surface, p-type Si/SiO_2 and mica, that were investigated by AFM. The two samples show rather different morphology patterns, that can be attributed to the different surface properties of the substrate, in turn affecting the polymeric complex assembly. In Fig. 5, the AFM morphology images of **1** deposited on Si/SiO_2 (Fig. 5a) and mica (Fig. 5b) are reported . It is worth to note that, whereas the Fe-complex self-assembles on Si/SiO_2 as typically observed for a polymeric species deposited onto a surface, with the formation of spherical grains (with a diameter ranging from 30 nm to 80 nm; Fig. 5a), a completely different pattern can be observed when the same solution is spin-coated onto freshly cleaved mica (Fig. 5b). In the latter case, a series of undulated ridges roughly aligned, as a sort of nanofibers, can be observed on the atomically flat surface of mica ((Fig. S2 and Fig. S3), that have a length ranging from some tens of nm to few hundred nm, and an average height of about 0.7 nm. Such a height value is compatible with the monolayer self-assembling of the polymeric species on the surface, as estimated by a simple molecular mechanics calculations of some Fe-oligomers.

The reason for such different self-assembling behavior of the Fe-polymeric complex onto mica, with respect to Si/SiO_2, can be attributed to the role played by the different surface interactions: while on the silica surface no preferential driving interaction occurs, on the surface of freshly cleaved mica cooperative ion-dipole interactions set up between the layer of K^+ cations left [27], on one side, and the chloride ligands and/or nitrogens of **tp** moieties, on the other. Thus, such an effect

allows to assembly a monolayer of the polymeric chains of the compound on the mica surface, at odd with the case of Si/SiO_2 that leads to an agglomeration of the Fe-complex oligomers to give sphere-like structures.

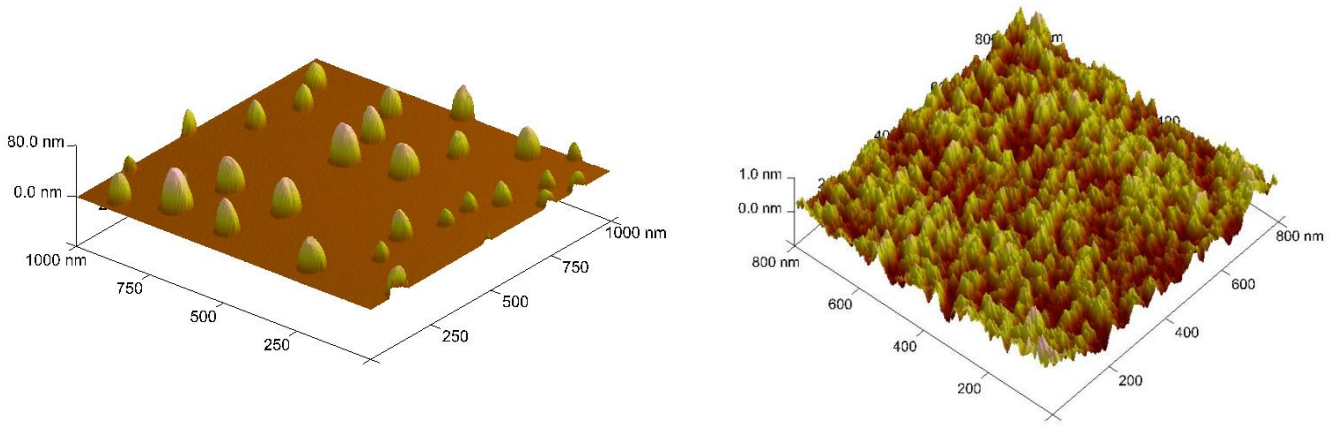

a **b**

Fig. 5 AFM morphology images of polymeric **1** spin-coated on (**a**) p-Si/SiO_2 and (**b**) freshly cleaved mica surface.

4. Conclusions

An iron(III) polymeric compound with [1,2,4]triazolo[1,5-*a*]pyrimidine (**tp**) ligand was synthesized and structurally characterized by spectroscopic methods; its redox properties, and the electrochemical mechanism it undergoes, were also investigated. The molecular structure of $[FeCl_3(\mathbf{tp})_2]_n$ (**1**) was investigated by single crystal X-ray diffraction method. The metallo-supramolecular coordination polymer, resulting from the self-assembly of metal and ligands, forms a ladder structure, stabilized by a network of H-bonding and stacking interactions into a 3D nanostructured material, with slightly more than 10% in volume open to host solvent or guest molecules. Interestingly, the coordination polymer structure is retained in solution, without any disassembling of the metallo-supramolecolar polymer into discrete molecular units as also

evidenced by DLS measurements. Interestingly, DLS measurements showed the presence of nano-aggregates in suspension, attributable to the coordination polymer structure, that is retained in solution, without the complete disassembling of the metallo-supramolecolar polymer into discrete molecular units. By this technique, a confirmation of the nanosized nature of these aggregates can be appreciated: the shape evaluation will be the object of future measurements carried out with multiangle LS instrumentation.

The hydrodynamic dimensions measured for solvated nano-objects of **1** is in agreement with that obtained for these structures determined by AFM in dry conditions.

In order to produce tailor-made metal nanoparticle materials of wide application starting from such versatile building blocks, the supramolecular assembly may be further and easily fine-tuned either generating opportune nanocavities by using ligands of different size as linkers between the iron atoms or by using its nanostructured morphology as a precursor towards a family of opportunely tailored iron nanowires or metal nanoparticles.

Finally, the proof of concept that such supramolecular polymeric coordination compound can be regarded as a nanowire structure has been provided by exploiting its interactions with the surfaces of freshly cleaved mica, as highlighted by the AFM morphological patterns.

Acknowledgements

P.S., S.D.A., J.I. and M.M. gratefully acknowledge the University of Bologna for financial support.

Appendix A. Supplementary data

CCDC **1830492** contains the supplementary crystallographic data for **1**. These data can be obtained free of charge via http://www.ccdc.cam.ac.uk/conts/retrieving.html, or from the Cambridge Crystallographic Data Centre, 12 Union Road, Cambridge CB2 1EZ, UK; fax: (+44) 1223-336-033; or e-mail: deposit@ccdc.cam.ac.uk. Supplementary data to this article can be found online at https://doi.....

Table 1. Crystal data and details of measurements

Crystal parameters	$[FeCl_3(\mathbf{tp})_2]_n$ (**1**)
Empirical formula	$C_{10}H_8N_8FeCl_3$
M /g mol^{-1}	402.43
Temperature (K)	293
Wavelength (Å)	0.71073
Crystal system	Monoclinic
Space group	*C2/c*
a (Å)	17.621(3)
b (Å)	9.060(1)
c (Å)	19.042(5)
β (°)	112.20(3)
Volume (Å^3)	2814.8(10)
Z	8
$\rho_{calc.}$ /g cm^{-3}	1.89
Crystal size (mm)	0.28×0.35×0.45
Crystal color	red
θ Range for data collection (°)	3 – 30
Index range	$-21 \le h \le 23$
	$-11 \le k \le 9$
	$-15 \le l \le 24$
Reflections collected	7092
Data/restraints/parameters	1638/0/200
Goodness-of-fit on F^2	0.927
Final R indices [$I > 2\sigma(I)$]	R_1 = 0.056
	wR_2 = 0.104
Largest diff. peak and hole (eÅ^{-3})	0.53 -0.54

Table 2. Selected bond distances (Å) and angles (°) with their e.s.d.s

	$[FeCl_3(\mathbf{tp})_2]_n$ **(1)**		
	A	**ave.**	**B**
Fe–Cl(1)		2.270 (1)	
Fe–Cl(2)		2.345 (1)	
Fe–Cl(3)		2.289 (1)	
Fe–N(1)			2.200(4)
Fe–N(3)	2.142(4)		2.270(4)
N(1)–C(2)	1.305(7)		1.322(6) 1.370(5)
N(1)–N(8)	1.378(5)		1.349(6)
C(2)–N(3)	1.374(6)		1.366(5)
N(3)–C(4)	1.357(6)		1.344(6)
N(4)–C(4)	1.335(6)		1.322(5)
N(4)–C(5)	1.324(6)		
Cl(1)-Fe–Cl(2)		173.5(1)	
Cl(1)-Fe–Cl(3)		93.4(1)	
Cl(3)-Fe-Cl(2)		92.7(1)	
N(3A)-Fe-N(1B)		174.5(1)	
N(3A)-Fe-N(3B)		85.5(1)	
N(1B)-Fe-N(3B)		89.2(1)	
N(3)-Fe-Cl(1)	92.3(1)		88.3(1)
N(1B)-Fe-Cl(1)		88.9(1)	
N(3)-Fe-Cl(3)	93.1(1)		177.8(1)
N(1B)-Fe-Cl(3)		92.1(1)	
N(3)-Fe-Cl(2)	89.6(1)		85.6(1)
N(1B)-Fe-Cl(2)		88.511)	
C7-N8-N1	126.8(5)		128.0(5)
C7-N8-C4	122.4(5)		122.1(4)
N1-N8-C4	110.7(4)		109.8(4)
C2-N1-N8	102.1(4)		102.8(4)
C5-N4-C4	113.9(5)		114.9(5)
N3-C4-N4	128.1(5)		128.4(5)
N3-C4-N8	108.3(5)		108.6(4)
N4-C4-N8	123.6(5)		122.9(4)

References

[1] J. M. Salas, M. A. Romero, M.P. Sánchez, M. Quirós, Coord. Chem. Rev. 193-195 (1999) 1119.

[2] (a) M. A. Girasolo, L. Canfora, P. Sabatino, D. Schillaci, E. Foresti, S. Rubino, G. Ruisi, G. Stocco, J. Inorg. Biochem. 106 (2012) 156;

(b) M. A. Girasolo, A. Attanzio, P. Sabatino, L. Tesoriere, S. Rubino, G. Stocco, Inorg. Chim. Acta 423 (2014) 168;

(c) I. Łakomska, M. Fandzloch, Coord. Chem. Rev. 327–328 (2016) 221, and references therein.

[3] D. Lipkind, N. Rath, J. Chickos, V.A. Pozdeev, S.P. Verevkin, J. Phys. Chem. B 2011,8, 8785-8796.

[4] A. K. Dutta, S. Biswas, S. Dutta, L. N. Dawe, C. R. Lucas, B. Adhikary, Inorg. Chim. Acta 444 (2016) 141.

[5] A. Y. Lukmantara, D. S. Kalinowski, N. Kumar, D. R. Richardson, J. Inorg. Biochem. 141 (2014) 43.

[6] A. Silvestri, G. Ruisi, M. A. Girasolo, J. Inorg. Biochem. 92 (2002) 171.

[7] (a) J. G. Haasnoot, D. W. Engelfriet, J. Reedijk, Inorg. Synth. 23 (1985) 157;

(b) P. Stupik, J. H. Zhang, M. Kwiecien, W. M. Reiff, J. G. Haasnoot, R. Hage, J. Reedijk, Hyperfine Interact. 28 (1986) 725;

(c) P. Stupik, W. M. Reiff, R. Hage, J. Jacobs, J. G. Haasnoot, J. Reedijk, Hyperfine Interact. 40 (1988) 343.

[8] H. L. C. Feltham, A. S. Barltrop, S. Brooker, Coord. Chem. Rev. 344 (2017) 26.

[9] (a) M. Biagini Cingi, A. M. Manotti Lanfredi, A. Tiripicchio, J. P. Cornelissen, J. G. Haasnoot, J. Reedijk, Inorg. Chim. Acta 127 (1987) 189;

(b) M. Biagini Cingi, A. M. Manotti Lanfredi, A. Tiripicchio, J. G. Haasnoot, J. Reedijk, Inorg. Chim. Acta, 101 (1985) 49.

[10] J. M. Balkaran, S. C. P. van Bezouw, J. van Bruchem, J. Verasdonck, P. C. Verkerk, A. G. Volbeda, I. Mutikainen, U. Turpeinen, G. A. van Albada, P. Gamez, J. G. Haasnoot, J. Reedijk, Inorg. Chim. Acta 362 (2009) 861.

[11] H. Liu, Y. Kou, L. Feng, D. Li, C. Gao, J. Tian, J. Zhang, S. Yan, Appl. Organomet. Chem. 24 (2010) 636.

[12] A. Winter, U. S. Schubert, Chem. Soc. Rev. 45 (2016) 5311, and references therein.

[13] A. J. M. Duisenberg, R. W. W. Hooft, A. M. M. Schreurs, J. Kroon, J. Appl. Crystallogr. 33 (2000) 893.

[14] A. J. M. Duisenberg, J. Appl, Crystallogr. 25 (1992) 92.

[15] G. M. Sheldrick, SADABS, University of Göttingen, Göttingen,Germany, 2004.

[16] G.M. Sheldrick, XPREP, Bruker-Nonius AXS, Madison, USA, 2005

[17] G. M. Sheldrick, Acta Crystallogr. C71 (2015) 3.

[18] G. M. Sheldrick, Acta Crystallogr. A64 (2008) 112.

[19] C. F. Macrae, P. R. Edgington, P. McCabe, E. Pidcock, G. P. Shields, R. Taylor, M. Towler , J. van de Streek, J. Appl. Crystallogr. 39 (2006) 453.

[20] a) B.J .Berne, R. Pecora (1976) Dynamic light scattering: with applications to chemistry, biology, and physics. Wiley, New York b) A Technical Note from Malvern Instruments: http://www.malvern. com/common/downloads/campaign/MRK656-01.pdfA.

[21] (a) C. Bruno, F. Paolucci, M. Marcaccio, R. Benassi, C. Fontanesi, A. Mucci, F. Parenti, L. Preti, L. Schenetti, D. Vanossi, J. Phys. Chem. B 114 (2010) 8585;
(b) A. Mateo-Alonso, G. Fioravanti, M. Marcaccio, F. Paolucci, G. M. A. Rahman, C. Ehli, D. M. Guldi, M. Prato, Chem. Commun. 0, (2007) 1945.

[22] C. Amatore, C. Lefrou, J. Electroanal. Chem. 324 (1992) 33.

[23] L. Mottier, Antigona program, University of Bologna, Bologna, Italy, 1999.

[24] L. Petrizza, D. Genovese, G. Valenti, M. Iurlo, A. Fiorani, F. Paolucci, S. Rapino, M. Marcaccio, Electroanal. 28 (2016) 2777.

[25] E. Szłyk, A. Grodzicki, L. Pazderski, E. Bednarek, B. Kamieński, Polyhedron 19 (2000) 965.

[26] H. Liu, N. Pierre-Pierre, Q.Huo Gold Bull (2012) 45:187–195 and references therein.

[27] P. Bampoulis, K. Sotthewes, M.H. Siekman, H. J.W. Zandvliet B. Poelsema, Sci. Rep.7 (2017) 43451.

Figure captions

Fig. 1 The asymmetric unit for **1**, showing the atomic crystallographic numbering scheme. Displacement ellipsoids are drawn at the 50% probability level. **(b**) Infinite chain of **1** as viewed along the *a* axis.

Fig. 2 Packing of **1**. In the close-up, right, head-to-tail π-stacking are shown.

Fig. 3 Size distribution curve for **1** by DLS analysis.

Fig. 4 Cyclic voltammetric curves of Fe-polymer in 0.1 M TBAH/ACN. T=25 °C; scan rate **(a)** 1 V/s, **(b)** 5 V/s.

Fig. 5 AFM morphology images of polymeric **1** spin-coated on (**a**) p-Si/SiO_2 and (**b**) freshly cleaved mica surface.

Graphical Abstract

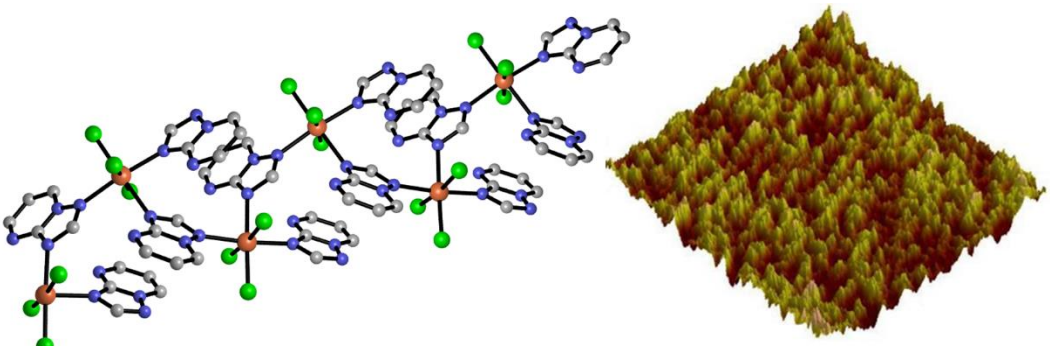

Graphical Abstract Synopsis

The coordination polymer resulting from the molecular assembly of metal and ligands forms a nanowire structure, as evidenced by X-Ray crystallography and AFM imaging. DLS measurements confirm its nanowire nature and exhibit a size of ca. 80 nm for one of the axis of the non-spherical nanostructures. Such a dimension for solvated nano-objects is in agreement with that of the dry structures determined by AFM.